A Hydrodynamic Study of a Fast-Bed Dual Circulating Fluidized Bed for Chemical Looping Combustion

Syed K. Haider,[a] Lunbo Duan,[a, c] Kumar Patchigolla,[b] and Edward J. Anthony*[a]

This study explores the use of a dual interconnected circulating fluidized bed (CFB) for chemical looping combustion. This design can enhance gas–solid interactions, but it is difficult to control the solid transfer and circulation rates. With the use of a 1:1 scale cold-flow model, an investigation determining the hydrodynamic behavior of the dual CFB system has been conducted. The cold-flow system consists of two identical fast-bed risers, each with an internal diameter of 100 mm and a height of 7 m. The simplified cold-flow model is based on the chemical looping Pilot-Scale Advanced CO_2 Capture Technology (PACT) facility at Cranfield. Here, we have determined the minimum fluidization and transport velocities, and we have assessed the solid density profiles, transport capacity, and potential for the dilution by air/N_2 leakage into the CO_2 stream exiting the fuel reactor. The experimental procedure uses two different bed materials, molochite (ceramic clay) and FE100 (iron particles), and it satisfies the dynamic scaling laws to model the bed inventory within the system. The results indicate that the two fast-bed risers share similar density and pressure profiles. Stable circulation can be achieved through pneumatic transport. The circulation rate of the system is flexible and can be adjusted by altering the fluidization velocity in the riser and by altering the bed inventory. The gas leakage from the loop seal to the cyclone was found to be sensitive to the bed height and fluidization velocity in the loop seal. However, by maintaining a loop-seal bed height above 600 mm during operation, the outlet stream remains undiluted.

Introduction

As a result of the industrial maturity of circulating fluidized-bed (CFB) reactors, the technology is widely deployed. In the power generation sector, the use of CFB boilers is particularly common, due to their ability to utilize low-grade, low-calorific-value fuels, and maintain the capability for flexible operation.[1] This flexibility lends itself well to other technologies, including high-temperature looping cycles for fossil fuel conversion and carbon capture systems.[2] A high-temperature solid looping process known as chemical looping combustion (CLC) is the focus of this work. Such high-temperature looping systems must first be demonstrated at smaller scales using pilot-scale systems. CFB systems must consider the physical properties of the particles used (e.g., density, size, melting point) and the relevant reaction chemistry, plus decide the range of operating temperatures, residence times and, ultimately, the optimum reactor configuration to be used. Though CLC systems are based on CFB principles and can utilize reactor configurations such as CFB packed/moving bed and CFB bubbling-bed variants, the use of dual interconnected CFBs with fast fluidized-bed operation can allow for greater gas–solid contact and could be beneficial for the CLC process. This reactor configuration and mode of operation poses difficulties in accurate control of the solid transfer and circulation rates. Therefore, it is necessary to use a cold-flow system that can accurately determine the fluid-dynamic properties presented by the fluidized particles and a given reactor configuration, while conducting tests at ambient conditions.

The operational and process considerations are explored here for a chemical looping combustor, for intended use with gaseous fuels and a copper(II) oxide-based oxygen carrier.[3] The focus of this study is to investigate the solids handling and solid control behavior of a chemical looping reactor by using a 1:1 scaled cold-flow model (CFM). A comprehensive hydrodynamic study, including bed height sensitivity analysis, will provide data to predict if continuous circulation can be maintained with stable operation.

[a] Dr. S. K. Haider, Dr. L. Duan, Prof. E. J. Anthony
Centre for Combustion, Carbon Capture and Storage
School of Energy, Environment and Agrifood
Cranfield University, MK43 0AL (UK)
E-mail: b.j.anthony@cranfield.ac.uk

[b] Dr. K. Patchigolla
Centre for Power Engineering
School of Energy, Environment and Agrifood
Cranfield University, MK43 0AL (UK)

[c] Dr. L. Duan
Key Laboratory of Energy Thermal Conversion and Control
Ministry of Education, School of Energy and Environment
Southeast University, Nanjing, 210096 (PR China)

Chemical looping combustion and fluidized beds

Lewis and Gilliland[4] were the first to study the concept of producing pure CO_2 from carbon-containing fuels by their reduction using a solid copper oxide as an oxygen source. It was later developed as a means for carbon capture and responsible fossil fuel conversion, and thus, a potential contributing strategy for climate change mitigation was developed by Ishida et al.[5]

Lyngfelt et al.[6] developed the first chemical looping reactor scheme based on the CFB principle. The technology's major benefit centers on its ability to convert fuel to combustion products in the absence of air, avoiding any post-combustion flue-gas treatment to separate the CO_2 along with its associated energy penalties.[7] CLC is a two-stage process by which oxygen is absorbed from air by a solid oxygen carrier (typically a transition metal oxide). The exothermic oxidation reaction takes place in a fast-bed riser known as the air reactor (AR). The high-velocity gas stream enters a cyclone where the oxygen carriers are separated from the oxygen-depleted air and sent to the fuel reactor (FR) to provide the oxygen required for combustion of the fuel, typically by an endothermic reaction process.[8] The reduced oxygen carrier is then returned to the AR to continue the cyclic process (see Figure 1).

The development and testing of potential oxygen-carrier materials is the most widely researched topic in the CLC field.[10] Oxygen carriers are usually transition metal oxides, namely nickel, copper, iron, and manganese.[8] Oxygen carrier research has investigated materials ranging from ores[11,12]
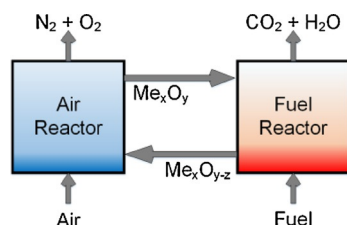

Figure 1. Simplified chemical looping process (adapted from Ref. [9]).

and industrial waste,[13] to combined metal oxides systems[14] and highly engineered nanostructured particles.[15] The current magnitude of chemical looping reactors installed ranges from $0.3–1000\ kW_{th}$ and spans different research groups that have achieved more than 4000 h of operational experience collectively.[16] The majority of this operational experience came from the conversion of gaseous fuels, although the use of solid and heavy liquid fuels is now the focus of current research.[17]

Several configurations of reactor design have been considered for CLC applications, the most common being the dual circulating fluidized-bed system for gaseous fuels. In systems utilizing solid fuels, such as coal and/or biomass, a third reactor will likely be added to the system to improve fuel conversion. Loop seals incorporated between the reactors prevent the reaction gases from mixing with one another. Adanez et al.[18] has reviewed various reactor configurations in detail. The commonly proposed reactor configurations and corresponding operating conditions are summarized in Table 1.

Dual fast-bed Cranfield design

The Cranfield Pilot-Scale Advanced CO_2 Capture Technology (PACT) chemical looping reactor comprises two identical interconnected CFBs known as the air and fuel reactors. The riser height of each reactor is 7.3 m with an inner diameter of 0.1 m. The two reactors lead to primary and secondary cyclones, which return solids to the appropriate reactor by way of a return leg (down-comer) with an inner diameter of 0.04 m. The reaction environments are designed not to mix and are separated by a loop seal (LS); this can help facilitate the solids throughput but is one-directional and, therefore, cannot be used as a long-term strategy for controlling the solid circulation. Figure 2 shows a diagram of the chemical looping reactor. The intended goal of this facility is to study the conversion of gaseous fuel (methane) in the fuel reactor using a re-circulating copper oxide-based oxygen carrier to demonstrate pilot-scale CLC processes.

Table 1. Reactor configurations and operation characteristics.

| Reactor pattern	Mode 1	Mode 2	Mode 3
operation regime	moving/packed bed	bubbling, turbulent or spouted fluidized bed	fast fluidized bed
gas/solid flow pattern	counter-current	mixed/co-current	mixed/co-current
gas/solid contact	low	high	high
fuel and OC conversion	high, but may be low when scaling up due to the poor mixing	may be low, due to back mixing and gas channeling	high by recirculation
solid circulation rate	low	medium	high
ash separation technique with solid fuel	easy	difficult	difficult
particle size (μm)	1000–3000	usually 100–1000, wide range is acceptable	usually 100–600, wide range is acceptable
gas velocity ($m\,s^{-1}$)	>1	2–4	2–6
temperature	<1100	<1100	<1100
reactor size	large	medium	medium–small
scale up	difficult	easy	easy
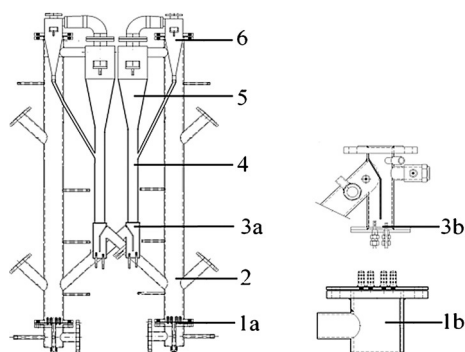
Figure 2. Cranfield dual interconnected CFB design (not to scale): 1a) Distributor nozzles, 1b) Wind box and magnified distributor nozzles, 2) Main riser, 3a) Loop seal, 3b) Loop-seal distributor nozzles, 4) Return leg, 5) Primary cyclone, 6) Secondary cyclone.

Requirement for operational strategy analysis

The design of a symmetrical system as described above has an inherent difficulty in operation with respect to controlling the solid circulation between the two reactors and heat management. With the assumption of no requirement for the additional make-up oxygen carrier material, maintaining stable and balanced operation requires the solid flow transferred from the AR to the FR (m2 in Figure 3) to be equal to the solids flow transferred from the FR to the AR (m1 in Figure 3). The difficulty in controlling this arises from the two different reactions occurring in the AR and FR. The transfer of solids would be determined by the temperatures of the reactors, specific particle properties (e.g., size, density, and sphericity), and the fluidizing gas properties such as density and viscosity.

To determine the best strategy for operation, a description of the heat and mass balance is presented below. The reactions considered include the conversion of methane using a copper-based oxygen carrier (60 wt% CuO and 40 wt% Al_2O_3), which reduces to Cu_2O under chemical looping with oxygen uncoupling (CLOU) processes. The following assumptions are also made: the formation of combustion products is stoichiometric with respect to the input fuel and, therefore, complete; all of the O_2 is consumed in the fuel re-
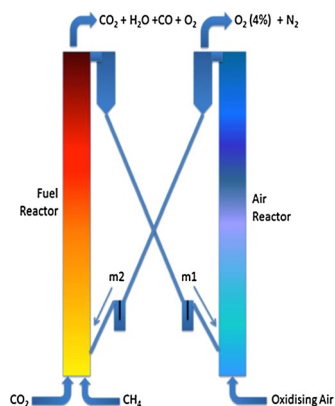
actor; no heat is transferred by the oxygen carrier support material, which is inert and considered equal in terms of mass in and out; and the particle size distributions in the two columns are assumed to be the same, even though the particle size may in fact change during the oxidation/reduction reactions as well as changing with time due to attrition.

With the pre-set design condition of 50 kW input based on the current configuration of electrical heating and the heat of combustion of methane, mass flowrates of 5.03 $Nm^3 h^{-1}$ for methane and 47.6 $Nm^3 h^{-1}$ for air are ideally required. In a hypothetical scenario assuming a bed temperature of 800°C and 4% excess air, the corresponding gas velocity to be expected in the AR is 5.48 $m s^{-1}$. Taking into account the differences in density of the flue gases in the AR (majority N_2) and in FR (CO_2 and H_2O) it is estimated that an additional 22.74 $Nm^3 h^{-1}$ of CO_2 is required to balance the solid transfer between the two reactors. It would be ideal to recycle the flue gas from the FR, but in practical operation of the system we can simply supply the additional required CO_2 to operate under equivalent fluidization conditions. An additional advantage to recycling of the CO_2 in this system is the decrease in the equilibrium partial pressure of oxygen in the fuel reactor. This further enhances the CLOU effect, in terms of release of gaseous oxygen from the copper-based oxygen carrier. With respect to the conversion ratio of the oxygen carrier, a circulation rate of 120–240 $kg h^{-1}$ is required for conversion ratios of 1 (CuO/Cu) and 0.5 (CuO/Cu_2O), respectively.

In the first case, the system as a whole (AR+FR) was considered in the heat and mass balance calculations. The input streams were air and methane, whereas the exit streams consisted of 4 vol% O_2 with the balance as N_2, CO_2, and H_2O. The bed temperature was set at 900°C. It was calculated that approximately 30 $kJ s^{-1}$ of heat is required to be removed from the system as a whole.

In the second case, the heat and mass balance of the AR and FR were treated separately. It was calculated that without CO_2 recycle the FR will require heat removal of 7.89 $kJ s^{-1}$. This can be somewhat reduced as it is possible to supply CO_2 at room temperature. It was calculated that 12.1 $kJ s^{-1}$ of heat would be required to heat up the CO_2, which could be supplied by the reactor external heaters. The situation for the AR is less simple, due to the strong exothermic reaction of the oxygen carrier oxidation, for which it was calculated that approximately 22 $kJ s^{-1}$ of heat must be removed. The dissipation of heat through the reactor walls can only account for 1 $kJ s^{-1}$ heat loss due to the two surrounding adiabatic furnaces. In the current configuration, there is no available heat surface from which to extract heat. The comparisons between the heat balance of the system as a whole and individually show an error of 1%. As a consequence of the limitations in heat dissipation and management, a feasible strategy is, therefore, to reduce the electrical heat input to 20 kW. This in turn reduces the heat to be removed to manageable levels. The approximate mass flow rates required are 19.2 and 2.01 $Nm^3 h^{-1}$ for air and methane, respectively. An excess of an additional 9.1 $Nm^3 h^{-1}$ of CO_2 is required to ach-

Figure 3. Simplified process flow diagram of the PACT CLC reactor.

ieve a sufficient gas velocity (2.66 m s^{-1}) to balance the solid transfer between the two reactors. This corresponds to an oxygen carrier circulation rate of approximately 3.4 kg m^{-2} s^{-1}.

Scaling and dimensionless parameters

The design of larger-scale fluidized beds can be investigated at smaller scales under ambient conditions through cold-flow modeling, permitting detailed fluid-dynamic investigations. Normally, their importance lies in the possibility of predicting the experimental conditions in the corresponding larger-scale system.[19] A CFM can be made of a transparent material (typically plastic or acrylic) that allows one to view the internal fluidization behavior and particle mixing. In the case of CLC, notable studies include those conducted by Kronberger et al.,[20] Pröll et al.,[21] Shuai et al.,[22] and Markström and Lyngfelt.[23]

The philosophy of cold-flow modeling utilizes non-dimensional analysis to provide scaling laws that can accurately represent dynamic similarity between a smaller-scale CFM and a corresponding larger reactor system. The non-dimensional analysis of system similarity was adapted and developed for fluidized beds by Glicksman,[24] in which he proposed a full set of scaling laws, allowing ambient temperature modeling of systems operating at elevated temperatures. These scaling laws were later simplified in Glicksman's 1993 study,[25] which presented a relaxed set of parameters [Eq. (1)]. These laws are appropriate for both viscous and inertial dominated regions of the fluidized bed, and are valid over a wide range of Reynolds numbers applicable to small particles at low fluidization velocities and large particles at high fluidization velocities, which was a limitation of his previously proposed scaling laws.

$$\frac{u_0^2}{gL}, \frac{\rho_s}{\rho_g}, \frac{u_0}{u_{mf}}, \frac{L_1}{L_2}, \frac{G_s}{\rho_s u_0}, \varphi \tag{1}$$

Glicksman's scaling laws are generally regarded as the standard methodology for scaling fluidized beds, and though many investigations have proven the applicability of these laws, limitations still exist. Examples of such limitations are the studies conducted by Pröll et al.[21] who determined that neither gas and particle wall friction effects, nor solid particle acceleration are accounted for. A review of scaling law limitations is presented by Cotton et al.[26] Scaling laws in CLC become challenging to apply, due to the typically high densities of fluidized oxygen carriers. The use of higher-density particles can eliminate the requirement for scaling down a cold-flow system, while still allowing for sufficient dynamic similarity in comparison with a CLC reactor. The applicability of these scaling laws for the modeling of the CLC reactor and CFM are discussed in the Experimental Section.

Results and Discussion

Minimum fluidization and transport velocities

The resistance co-efficient of the riser gas distributor was measured by determining pressure drops above and below the distributor with varying gas velocities. Once this had been determined, the riser was filled with solid particles to a bed height of 550 mm. A step-wise increase in gas velocity (upstream) was applied to the bed material until fluidization was observed and then decreased step-wise (downstream). The pressure curves for the molochite and the FE100 particles are shown in Figure 4 and Figure 5, respectively. The downstream curves were utilized to determine the U_{mf} values (variables are defined in the definition list at the end of the article), which were estimated as 0.11 and 0.023 m s^{-1} for the molochite and FE100 particles, respectively. It was observed that there is a clear and noticeable difference when comparing the upstream curves of the two particles. Whereas molochite displays smooth transition into fluidization, the FE100 particles show an overshoot of pressure drop upon transitioning into the incipient fluidizing regime. This was also visually observed by a sudden increase in bed height in the upstream, whereas a smooth transition was observed when decreasing the fluidizing gas velocity. The pronounced hysteresis shown in Figure 5 is indicative of Geldart group A particles which
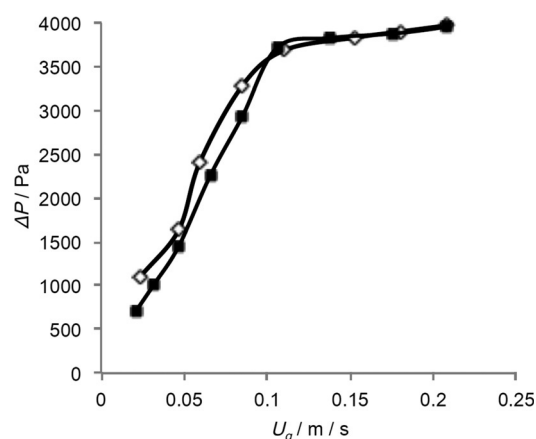

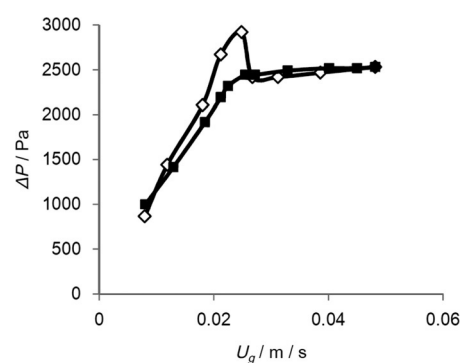**Figure 4.** Minimum fluidization velocity of molochite.

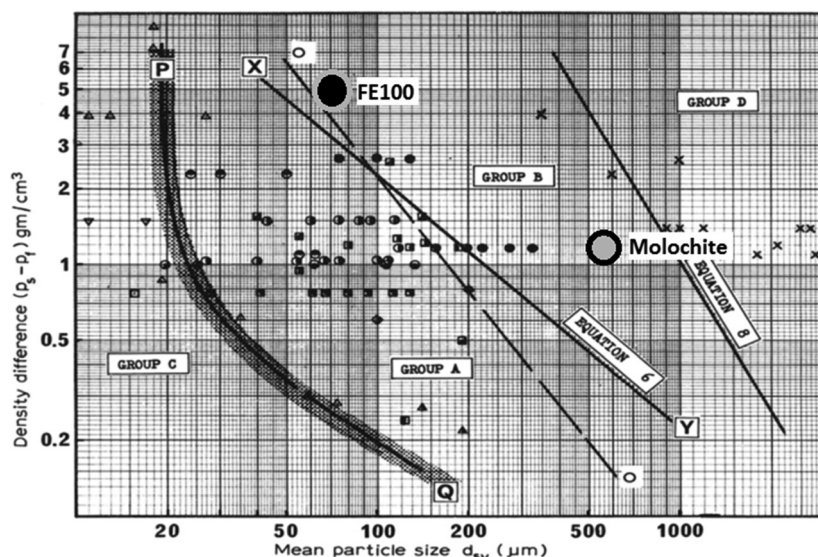**Figure 5.** Minimum fluidization velocity of FE100.

Figure 6. Geldart particle classification of molochite and FE100 (Adapted from Ref. [27]).

typically exhibit greater particle–particle cohesion.[27] The specific positions of the molochite and FE100 particles employed in this study in the context of their Geldart classifications are shown in Figure 6, and it was observed that although both classifications define the particles as group B, FE100 particles are located in close proximity to the particle A/B border and exhibit group A properties with respect to particle cohesion. The transport velocity U_{tr} was determined by visual observation of particles dropping from the cyclone to the return leg, coupled with the pressure drop of the bed; the transport velocities were determined to be 1.70 and 1.38 m s^{-1} for molochite and FE100, respectively.

Density profiles at varying velocities

The density profiles with varying fluidization velocities for molochite and FE100 are shown in Figure 7 and Figure 8, respectively. The general trends, with both particles employed,

are that the solid concentration (ξ_s) decreases as the height of the riser increases. In the case of molochite, at velocities below U_{tr}, the solid concentration is near 0.55, similar to that in a bubbling bed. As the gas velocity increases, the molochite particles are increasingly carried out of the bed and enter the freeboard. At velocities just above U_{tr}, (1.7 and 1.9 m s^{-1}) at a height of 0.45 m, the bed has a greater solid concentration (0.1) than the solid concentration of 0.07 corresponding to increased fluid gas velocities (≥ 2.1 m s^{-1}). At a height of 0.75 m, this solid concentration decreases for velocities close to U_{tr} indicating that in this region most particles are already elutriated.

In the case of the FE100 particles, the elutriation zone is higher than that of molochite. At a height of 0.75 m the bed has a greater solid concentration for velocities greater than U_{tr}, and the particles are carried out of the dense phase at greater height between 0.75 and 2 m. This could be attributed to the shorter static bed height where the gas hold-up is
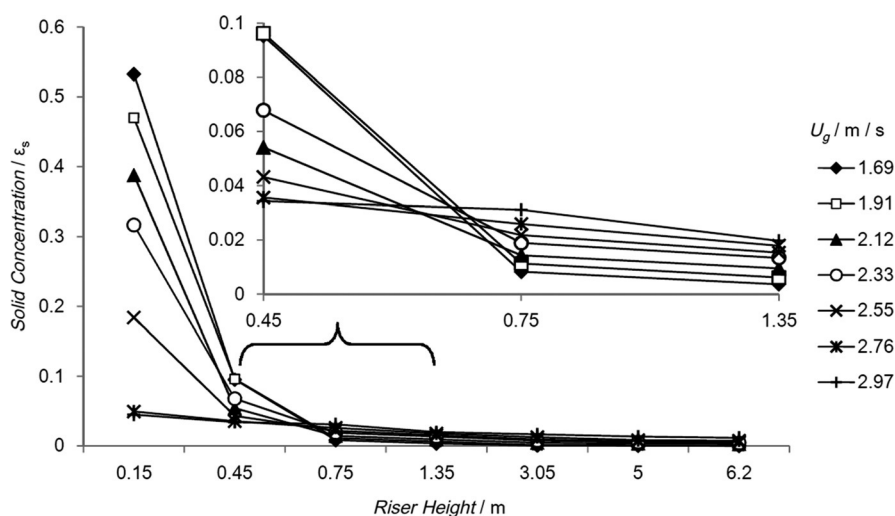

Figure 7. Density profiles at varying fluidization velocities (molochite static bed height = 550 mm).

© 2016 The Authors. Published by Wiley-VCH Verlag GmbH & Co. KGaA, Weinheim
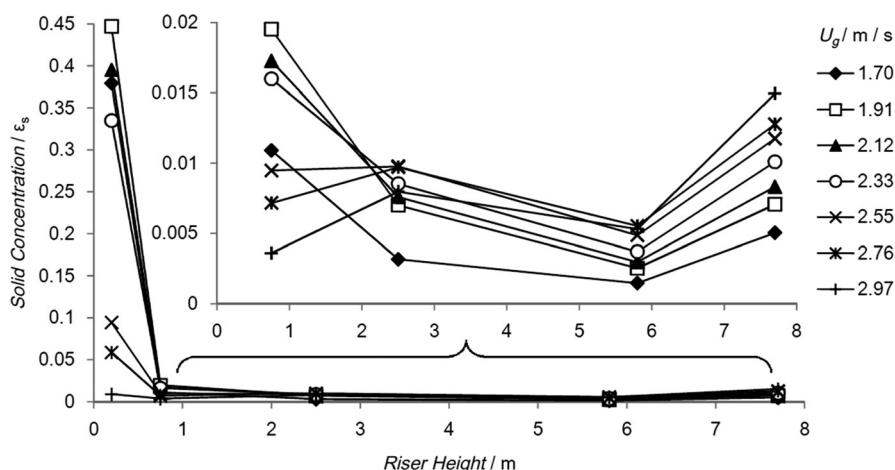
Figure 8. Density profiles at varying fluidization velocities (Fe100 static bed height = 230 mm).

limited in shorter beds. The density profile of FE100 shows an increase in density at the very top of the riser. Due to the high density and small diameters of the particles, the wall effects became important at this height as particles hit the top of the riser before being finally being carried through to the cyclone.

The pressure profiles of both the AR and FR risers under steady state conditions are shown in Figure 9. It was observed that for varying fluidizing velocities, the pressures in both reactors are very similar. This indicates that the solid exchange between the two reactors can be maintained in a stable operation despite the fact that the solid handling is controlled through pneumatic transport.

Solid circulation rate

The effects of varying static bed height and fluidizing velocity on the solid circulation rate were investigated for molochite and FE100 particles and are shown in Figure 10 and Figure 11, respectively. Typical behavior is observed, with the particle transfer rate increasing with greater gas velocity. In
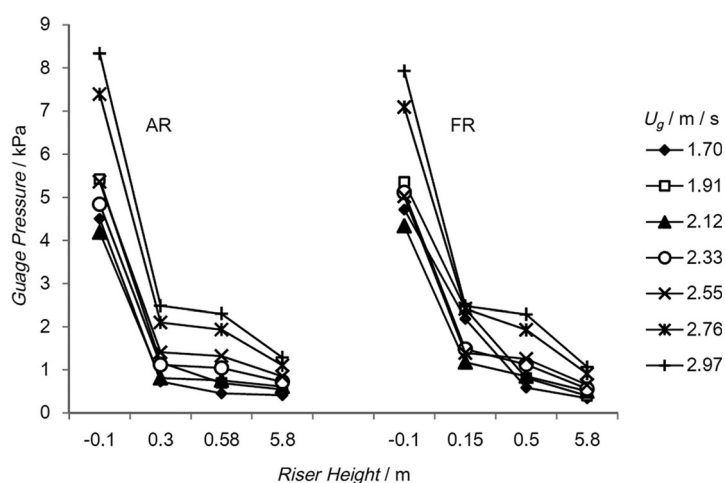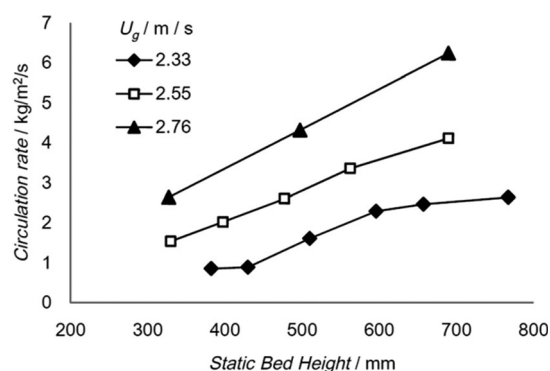

Figure 10. Solid transfer rate with varying velocity and static bed height (molochite).

the case of molochite, for a static bed height of 500 mm and a gas velocity increase from 2.33 to 2.76 m s^{-1}, the transfer of solids increases from 1.66 to 4.32 kg m^{-2} s^{-1}. With higher fluidizing velocities (2.55–2.76 m s^{-1}) the increase in solid transfer rate is fairly linear. Conversely, at lower velocities and a bed height varying from 600 to 770 mm the increase in rate of solids transferred is minimal, with a rise of 0.3 kg m^{-2} s^{-1}. At a velocity in the range of 2.55–2.76 m s^{-1} the bed circulation appears to be sensitive, when the bed height is in the region of 430–600 mm, for which the difference in solids transferred is 1.4 kg m^{-2} s^{-1}.

The FE100 particles followed the expected trend of increasing solids transfer with increasing fluidizing velocity. At lower velocity (2.33 m s^{-1}) the difference between the solids transferred with increasing static bed height from 200–450 mm was minimal and exhibited a rise of 1.8 kg m^{-2} s^{-1}. The rise in solid transfer with greater static bed height is greater for fluidizing velocities between 2.33 and 2.97 m s^{-1}. The dependence of increasing fluidizing gas velocity and a larger static bed yields an average rise of 6.4 kg m^{-2} s^{-1}. These results indicate that the circulation rate can be controlled in the dual

Figure 9. Pressure profile of both risers at steady state (static bed height = 550 mm).
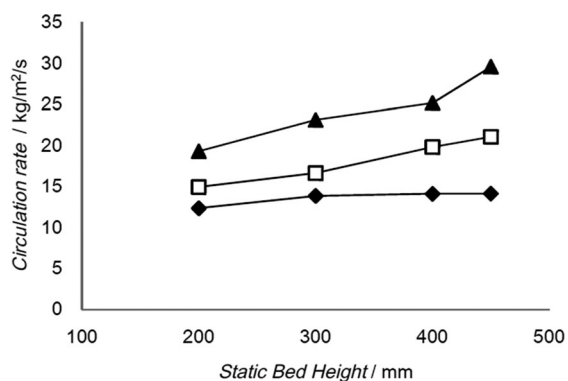
Figure 11. Solid transfer rate with varying velocity and static bed height (FE100).

CFB system by adjusting the fluidizing velocity, though the recirculation rate can also be increased by adding further bed material. This scenario is not ideal due to the thermal losses and energy penalty of adding cold particles for "hot" operation and the requirement of an increased pressure head in the wind-box.

Gas bypass leakage

For the chemical looping fast-bed reactor design it is essential to ensure that almost pure CO_2 is obtained at the exit of the FR cyclone. Gas bypass or leakage that dilutes this CO_2 stream can potentially increase the cost of CO_2 purification and separation. Therefore, the potential for gas leakage and methods for its reduction are important considerations. In this design, leakage can occur by gas passing in either a co-current or counter-current flow to the solids stream between the loop seal and cyclone connection. As air is used as the primary fluidizing gas in the CFM, the leakage ratio [Eq. (2)] was determined by introducing CO_2 as a trace gas to be monitored, where CO_2 replaced air as the fluidizing gas in the outlet of the FR loop seal. The leakage ratio can then be determined in terms of the amount of CO_2 detected in relation to the flowrate of CO_2 fluidizing the loop seal. Figure 12
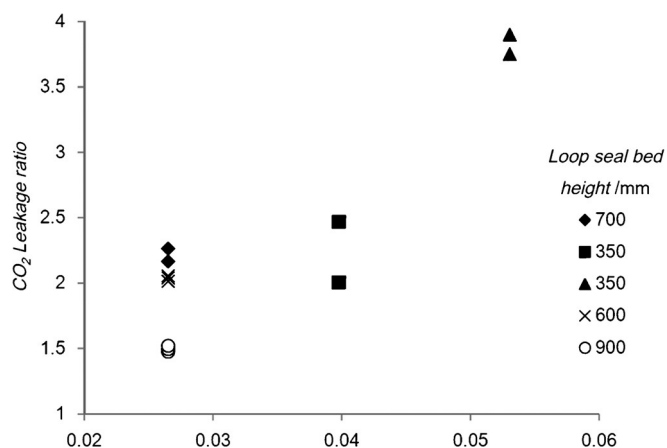

Figure 12. Leakage ratio with varying fluidizing gas velocity and loop-seal bed height.

shows the gas leakage ratio with FE100 particles, where the main considerations for investigation were the loop-seal fluidizing gas velocity and the bed height above the loop seal in the return leg. The riser flow rates were kept constant at 1000 L min^{-1} (2.12 m s^{-1}). During maintained stable and balanced operation, the system shows that CO_2 concentration at the exit of the FR cyclone can be maintained at a very low level. When the loop-seal fluidizing velocity is maintained below 0.05 m s^{-1} the system exhibits a leakage ratio of up to 2.5, corresponding to a CO_2 concentration of 0.7% with a minimal loop-seal bed height of 350 mm. The leakage ratio increases dramatically to 3.75–3.9, equivalent to a CO_2 concentration of 1.5–1.6%, upon increasing the loop-seal fluidizing velocity from 0.04 to 0.055 m s^{-1}. This indicates that, at this bed height, the system is sensitive to the fluidizing gas flow and velocity. These results indicate that the loop-seal bed height must be maintained above 600 mm to minimize the gas leakage from the riser. As presented in Figure 12, maintaining the loop-seal bed height above 600 mm results in CO_2 concentrations of 0.5%, which cannot be accommodated given the limits of the analysis methods employed here, and indicates that it is critical to avoid dilution of the stream exiting the FR reactor by maintaining an acceptable bed height. The investigation provides acceptable indicators for gas leakage control for transfer to the dual fast-bed system.

Conclusions

This investigation centers on the design philosophy of a 1:1 scale cold-flow model (CFM) for a dual interconnected circulating fluidized-bed system for the chemical looping combustion of gaseous fuels. The dual CFB system for chemical looping combustion allows for greater gas/solid contact compared to other reactor configurations, but it is difficult to control the transfer and circulation rate of the fluidized bed material. The use of a CFM allows the investigation of the fluidizing properties that can influence the rates of circulation and transfer at ambient conditions, with clear observations of the fluidizing behavior. The CFM was operated with two different particles (molochite and FE100) as bed material for a comprehensive understanding of the system hydrodynamic characteristics. The cold-flow system is modeled on the dual interconnected CFB fast-bed design of Cranfield's PACT facility chemical looping reactor. The major findings there are detailed as follows:

- The solids transfer between the dual CFB reactors can be controlled and maintained to a high level of stable operation in spite of the control philosophy governed by pneumatic transport.
- The circulation rate can be flexibly controlled by using the fluidizing gas velocity in the riser. The experimental investigation determines that the recirculation rate can also be adjusted through solid make-up of the bed inventory.

- Gas leakage investigations have shown that the dilution of the output stream from the FR cyclone can be minimal if stringent control of the loop-seal bed height is maintained above 600 mm.

Experimental Section

Cold-flow model design

Cold-flow model reactors are typically reduced in size compared to the larger reactors, which they aim to simulate based on Glicksman's dimensionless scaling laws. The CFM described in this investigation is of 1:1 scale to the Cranfield CLC fast-bed design. With this fast mode of fluid bed operation, it is necessary to reduce the possible gas/particle wall friction effects, which may have been unavoidable had the model been decreased in scale. This approach of "like-for-like" scaling has been successfully employed previously by Bischi et al.[29,30]

With the requirement for a 1:1 CFM plus the constraint of air being used as the fluidizing gas at this scale, it was necessary to satisfy other dynamically similar properties in Glicksman's simplified scaling laws. The conditions of the CLC unit with CFM are detailed in Table 2. The major parameters that were used to simulate similar dynamic properties between the two systems were the particle density and particle diameter. Metallic iron particles (FE100) from William Rowland UK and molochite ceramic particles from Imerys supplied by Castree Kilns were determined to be suitable bed materials for use in this investigation. The simplified scaling laws shown in Table 3 were applied using the conditions from Table 2, and it was determined that it was possible to obtain sufficient dynamic similarity and maintain reliability. This serves to allow one to utilize the CFM to control the solid flow, determine how much of the solids can be transferred in a given time, and determine how to avoid leakage. Then, by using the scaling criteria, one can determine the circulation rate (G_s) in the CLC reactor. The G_s of the CLC unit was calculated from the solids required, based on 20 kW operational input heat as a base case requirement for the operation of the CFM. For the modeling of CLC reactors, the AR and FR have different operational requirements. In the system described here, the only feasible operational strategy requires the balance of solids transferred between both reactors, which is achieved through CO_2 re-

cycle in the FR. As a consequence, the AR and FR are maintained under the same conditions in this study.

Analysis methods

Twenty GMH-Greisinger GMUD MP-S MR-1 model transducers were used to measure the pressures in this investigation. The pressure outlet taps were located in the wind box, the inlet and outlet of the loop seals, the outlet of the cyclone, the outlet of the riser, and at every 0.3 m interval up the length of the riser. These are often interchanged throughout the course of the investigation, and the heights at which they are located relative to above the wind-box distributor are detailed. These measurements are recorded using a TC-08 data-logger from Pico Industries and accompanying software suite for process monitoring.

Experimental procedures

The pressure data provided by the pressure transducers located in the dense bed, transition zones, up the length of the risers, the wind-box, and the outlet of the fluidizing gas inlet for the loop seals allowed for the determination of minimum fluidization velocity (U_{mf}), transport velocity/fast fluidization (U_{tr}) and the density profiles in the system. The solid circulation rate (G_s, $kg\,m^{-2}\,s^{-1}$) calculated at varying static bed heights was measured during stable fluidization, and then the fluidizing gas was cut off from the loop seals. The bed height of the accumulated solids in the return leg above the loop seal was measured over a short period of time. The reactor-to-reactor bypass leakage was determined by introducing CO_2 as a trace gas to the inlet of the fuel reactor loop seal and measuring any corresponding trace CO_2 at the outlet of the fuel reactor cyclone. This was measured by using a pre-calibrated ADC MGA 3000 multi-gas analyzer with

Table 3. CFM similarity with Glicksman scaling laws.

Condition	CLC Unit	CFM with FE100	CFM with molochite
U_0/U_{mf}	66	206	13
ρ_s/ρ_g	5733	4840	1165
$U^2_0/(gD)$	4.08	4.08	4.08
$G_s/(\rho_s U_0)$	9.17×10^{-4}	9.17×10^{-4}	9.17×10^{-4}

Table 2. Operational conditions of CLC vs. CFM.

Condition	CLC Unit	CFM with FE100	CFM with molochite
temperature (K)	1123	293	293
solid density, ρ_s ($kg\,m^{-3}$)	1800	5818	1400
gas density, ρ_g ($kg\,m^{-3}$)	0.314	1.202	1.202
gas viscosity, μ (Pa s)	4.50×10^{-5}	1.82×10^{-5}	1.82×10^{-5}
particle diameter, dp ($\times10^{-6}$ m)	300	60	519
U_{mf} ($m\,s^{-1}$)	0.03	0.01	0.16
pressure (atm)	1	1	1
inner diameter, D (m)	0.1	0.1	0.1
fluidization velocity, U_0 ($m\,s^{-1}$)	2	2	2
$U_{mf}/(gD)^{0.5}$	0.031	0.01	0.161
$Fr = (U_0-U_{mf})/(gD)^{0.5}$	1.99	2.01	1.86
dp/D ($\times10^3$)	3.000	0.6	5.19
G_s ($kg\,m^{-2}\,s^{-1}$)	3.3	2.56	10.7
ρ_g/ρ_s ($\times10^4$)	1.7	2.1	8.6
$Re = \rho_g U_0 dp/\mu$	4.2	7.1	68.5
$Ar = \rho_g \times (\rho_s-\rho_g) \times g \times (dp^3)/\mu^2$	74	45	6961

a CO_2 range of 0–40%. The CO_2 leakage ratio (LR_{CO_2}) is defined as Equation (2). P_{CO_2} is the measured CO_2 at the analysis point (vol%), Q_{riser} is the flowrate in the riser ($L m^{-1}$), and Q_{LS} is the flowrate of CO_2 in the loop seal ($L m^{-1}$). The leakage ratio was used to measure any possible dependence on the leakage with loop-seal bed height.

$$LR_{CO_2} = P_{CO_2} \bullet Q_{riser} \frac{100}{Q_{LS}} \qquad (2)$$

Nomenclature

Ar	Archimedes number
D [m]	internal diameter
dp [$*10^{-6}$ m]	particle diameter
Fr	Froude number
g [m s^{-2}]	gravitational acceleration
G_S [kg m^{-2} s]	solid circulation rate
L [m]	length of riser
LR_{CO_2}	CO_2 leakage ratio
P_{CO_2} [vol%]	CO_2% at analysis point
Q_{riser} [L m^{-1}]	flow rate in riser
Q_{LS} [L m^{-1}]	flow rate in loop seal
Re	Reynolds number
U_0 [m s^{-1}]	superficial fluidization
U_{mf} [m s^{-1}]	minimum fluidization velocity
U_{tr} [m s^{-1}]	transport velocity

Greek Letters

Δp [Pa]	pressure drop
ξ_S	solid concentration
φ	particle sphericity
μ [Pa s]	gas viscosity
ρ_g [kg m^{-3}]	gas density
ρ_s [kg m^{-3}]	solid density

Abbreviations

AR	air reactor
CFB	circulating fluidized bed
CFM	cold-flow model
CLC	chemical looping combustion
FR	fuel reactor
LS	loop seal
OC	oxygen carrier
PACT	Pilot-Scale Advanced CO_2 Capture Technology

Acknowledgements

[1] J. Koornneef, M. Junginger, A. Faaij, *Prog. Energy Combust. Sci.* **2007**, *33*, 19–55.
[2] E. J. Anthony, *Ind. Eng. Chem. Res.* **2008**, *47*, 1747–1754.
[3] L. Duan, D. Godino, V. Manovic, F. Montagnaro, E. J. Anthony, *Energy Technol.* **2016**, *4*, 1171–1178.
[4] W. K. Lewis, E. R. Gilliland, *Production of Pure Carbon Dioxide*, US 2,665,972, **1954**.
[5] M. Ishida, D. Zheng, T. Akehata, *Energy* **1987**, *12*, 147–154.
[6] A. Lyngfelt, B. Leckner, T. Mattisson, *Chem. Eng. Sci.* **2001**, *56*, 3101–3113.
[7] J. Wang, E. J. Anthony, *Appl. Energy* **2008**, *85*, 73–79.
[8] A. Abad, J. Adánez, F. García-Labiano, L. F. de Diego, P. Gayán, J. Celaya, *Chem. Eng. Sci.* **2007**, *62*, 533–549.
[9] T. Mattisson, A. Lyngfelt, P. Cho, *Fuel* **2001**, *80*, 1953–1962.
[10] Q. Imtiaz, D. Hosseini, C. Müller, *Energy Technol.* **2013**, *1*, 633–647.
[11] S. K. Haider, G. Azimi, L. Duan, E. J. Anthony, K. Patchigolla, J. E. Oakey, H. Leion, T. Mattisson, A. Lyngfelt, *Appl. Energy* **2016**, *163*, 41–50.
[12] H. Leion, T. Mattisson, A. Lyngfelt, *Energy Fuels* **2009**, *23*, 2307–2315.
[13] A. Fossdal, E. Bakken, B. A. Øye, C. Schøning, I. Kaus, T. Mokkelbost, Y. Larring, *Int. J. Greenhouse Gas Control* **2011**, *5*, 483–488.
[14] M. Rydén, H. Leion, T. Mattisson, A. Lyngfelt, *Appl. Energy* **2014**, *113*, 1924–1932.
[15] S. Bhavsar, M. Najera, R. Solunke, G. Veser, *Catal. Today* **2014**, *228*, 96–105.
[16] A. Lyngfelt, *Oil Gas Sci. Technol. Rev. IFP Energies nouvelles* **2011**, *66*, 161–172.
[17] P. Moldenhauer, M. Rydén, T. Mattisson, A. Hoteit, A. Jamal, A. Lyngfelt, *Energy Fuels* **2014**, *28*, 5978–5987.
[18] J. Adanez, A. Abad, F. Garcia-Labiano, P. Gayan, L. F. de Diego, *Prog. Energy Combust. Sci.* **2012**, *38*, 215–282.
[19] S. Shrestha, B. Si, M. Diana, B. Hamid, *Renewable Sustainable Energy Rev.* **2016**, *53*, 1529–1548.
[20] B. Kronberger, A. Lyngfelt, G. Lo, H. Hofbauer, *Ind. Eng. Chem. Res.* **2005**, *44*, 546–556.
[21] T. Pröll, K. Rupanovits, P. Kolbitsch, J. Bolhàr-Nordenkampf, H. Hofbauer, *Chem. Eng. Technol.* **2009**, *32*, 418–424.
[22] W. Shuai, L. Guodong, L. Huilin, C. Juhui, H. Yurong, W. Jiaxing, *Fuel Process. Technol.* **2011**, *92*, 385–393.
[23] P. Markström, A. Lyngfelt, *Powder Technol.* **2012**, *222*, 182–192.
[24] R. Glicksman, *Chem. Eng. Sci.* **1984**, *39*, 1373–1379.
[25] L. R. Glicksman, M. R. Hyre, P. A. Farrell, *Int. J. Multiphase Flow* **1994**, *20*, 331–386.
[26] A. Cotton, K. Patchigolla, J. E. Oakey, *Powder Technol.* **2013**, *235*, 1060–1069.
[27] D. Geldart, *Powder Technol.* **1973**, *7*, 285–292.
[28] E. Johansson, A. Lyngfelt, T. Mattisson, F. Johnsson, *Powder Technol.* **2003**, *134*, 210–217.
[29] A. Bischi, Ø. Langørgen, J.-X. Morin, J. Bakken, M. Ghorbaniyan, M. Bysveen, O. Bolland, *Energy Procedia* **2011**, *4*, 449–456.
[30] A. Bischi, Ø. Langørgen, J. X. Morin, J. Bakken, M. Ghorbaniyan, M. Bysveen, O. Bolland, *Appl. Energy* **2012**, *97*, 201–216.